

Supporting Information

Unraveling high-pressure gas storage mechanisms in shale nanopores through SANS

Rui Zhang^{1,†}, Shimin Liu^{1,*}, Long Fan¹, Tomasz P. Blach², and Guijie Sang^{1,‡}

¹Department of Energy and Mineral Engineering, G³ Center and Energy Institute, Pennsylvania State University, University Park, PA 16802, USA

²School of Minerals and Energy Resources Engineering, University of New South Wales, Sydney, NSW 2052, Australia

[†]Present address: Chemical Sciences Division, Oak Ridge National Laboratory, Oak Ridge, TN 37831, USA

[‡]Present address: Department of Civil and Environmental Engineering, University of Strathclyde, Glasgow G1 1XQ, UK

*Corresponding author: Shimin Liu, szl3@psu.edu

Pore structure evolution due to gas pressurization

To characterize the nanopore structure evolution under different pressure conditions for the shale samples, we have applied a global scattering function integrated Guinier approximation and power-law scattering, a unified scattering model, for data-fitting, in which the unified scattering model is superior to differentiate multiple structures in multiscale in a hierarchical porous medium. The method has been successfully used in shale in previous studies ^{1, 2}. The fitting of each scattering profile was conducted using SasView ³. The unified scattering equation without considering background can be expressed as ⁴

$$I(Q) = G \exp(-Q^2 R_g^2/3) + B(Q^*)^{-P} \quad (\text{S1})$$

$$Q^* = Q[\text{erf}(QR_g/\sqrt{6})]^{-3} \quad (\text{S2})$$

where the first term in Eq. S1 is Guinier's exponential form, and the second term is the structurally limited power-law form. Q^* is the modified scattering vector Q containing a three-dimensional Gaussian probability function, which accounts for the finite structural effect in the power-law region. G is the classic Guinier prefactor; R_g is the radius of gyration describing the domain size; B is the power-law prefactor; and P is the power-law exponent. The unified scattering model in Eq. S1 can be extended to describe multiple interrelated structural levels over a broad range of Q ⁴

$$I(Q) = \sum_{i=1}^n [G_i \exp(-Q^2 R_{g_i}^2/3) + B_i \exp(-Q^2 R_{g_{i+1}}^2/3) \times (Q^*)^{-P_i}] \quad (\text{S3})$$

$$Q^* = Q[\text{erf}(QR_{g_i}/\sqrt{6})]^{-3} \quad (\text{S4})$$

where i is the structural level, in which $i = 1$ refers to the largest-size structural level. According to the apparent configuration of the scattering profiles (Figs. 2, S2, and S4), the unified model with two structural levels was used to fit the scattering profiles for the Marcellus shale and Longmaxi shale samples, while the one with three structural levels was used to fit the scattering profiles for

the Illinois shale sample. Although the fitting was good for each scattering profile, the Guinier approximation at the largest-size structural level may not be reasonable because of the limited low Q measured. Fig. S8 shows the model fitting of the scattering profile under vacuum condition for each sample. The fitting parameters of all the scattering profiles are shown in Tables S3-S5.

Fig. S9 shows the power-law exponents as a function of pressure for each shale sample. Note that for mass or volume (pore) fractals, P is smaller than 3, in which $P = D_m(D_p)$. Thus, $D_m(D_p)$ is also smaller than 3⁵. For surface fractals, P is between 3 and 4, in which $P = 6 - D_s$. Thus, D_s is between 2 and 3. The integer D_s of 2 describes the situation of smooth surface. Additionally, for “fuzzy” interfaces, P is between 4 and 5, in which D_s lies between 1 and 2⁶. We can see that the P of structural level 1 for both the Marcellus shale and Longmaxi shale samples lies in the surface fractal region under vacuum condition. The value of P in structural level 1 decreases with increasing pressure over the entire range, indicating the increase of surface fractal dimension in large nanopores for both samples (Fig. S9a and b). The results are dramatically different from those in low-pressure region⁵. However, the value of P becomes smaller than 3 when the pressure is equal to or higher than 400 bar for the Marcellus shale sample. It suggests a transition from surface fractal to mass or volume (pore) fractal with increasing gas pressure in large nanopores for the sample. Interestingly, the P value of the structural level 2 for both the Marcellus shale and Longmaxi shale samples first decreases at initial pressure steps and then slightly increases at further pressure steps even when the two shale samples have different fractal characteristics under vacuum condition: mass fractal for the Marcellus shale sample and surface fractal for the Longmaxi shale sample (Fig. S9a and b). The result suggests a transition from surface fractal to mass fractal with increasing pressure in small nanopores for the Longmaxi shale sample this time. For the Illinois shale sample with the highest TOC among the samples measured, the value of P

seems pressure-independent in large and medium nanopores. Unlike the other two samples, the Illinois shale sample is mass fractal in large nanopores while surface fractal in medium nanopores (Fig. S9c). The value of P is close to 4, indicating a smooth surface in the middle-sized pore region for Illinois shale. Notably, we do not show the value of P in the structural level 3 for the Illinois shale sample as a function of pressure because of unreasonable fitted results for P under pressure conditions. It could be because of high uncertainty at the high Q region and small Q range for the fitting of the smallest-size structural level. But we do have a reasonable result of P under vacuum condition, which is 3.3, indicating surface fractal in small nanopores for this Illinois sample.

The estimated radius of gyrations for the shale samples are shown in Fig. S10. We do not show the values of R_g in the structural level 1 or the largest-size structural level for the shale samples, which may not be reasonable due to the limited low Q measured. For the Marcellus shale and Longmaxi shale samples (Fig. S10a and b), R_g does not have a global trend a function of pressure except that there is a linear correlation between R_g and pressure (0-30 MPa) for the Longmaxi shale sample. The domain size of the structure with smaller pores (structural level 2) does not have a globally either increasing or decreasing change as a function of gas pressure, indicating no selective gas injection in pores with different sizes. However, R_g may globally decrease with increasing pressure in the structural level 2, the medium-size structural level, for the Illinois shale sample, although the error bar is high (Fig. S10c). R_g in the smallest-size structural level has a sudden decrease after the initial pressure step and then becomes constant and has a slight increase with increasing pressure furtherly for the Illinois shale sample (Fig. S10d). It might suggest that selective gas invasion occurred in pores, which could be due to adsorption.

Figures

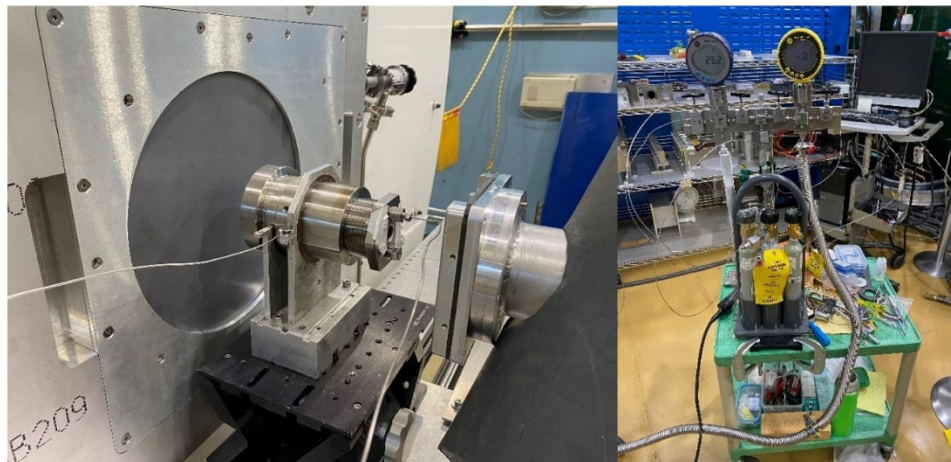


Figure S1 Photos of (left) the high-pressure cell on the vSANS beamline and (right) the portable gas intensification apparatus

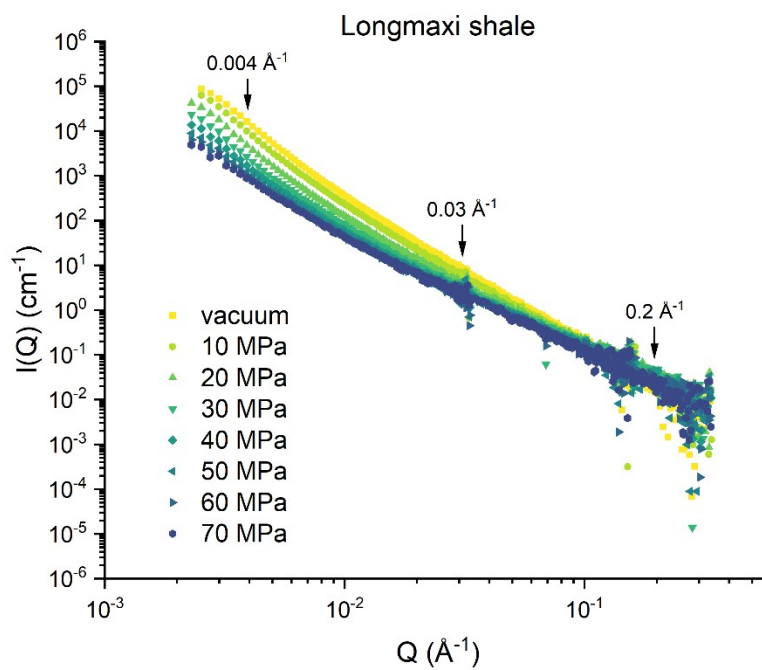


Figure S2 Scattering intensity as a function of methane pressure for the Longmaxi shale sample

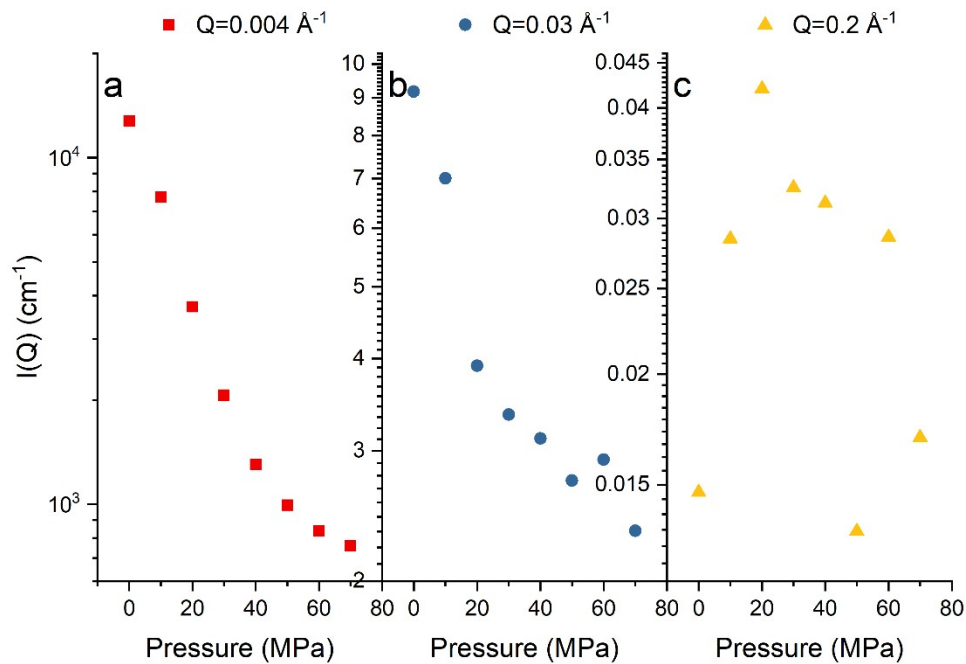


Figure S3 Scattering intensity as a function of methane pressure at (a) Q of 0.004 \AA^{-1} , (b) Q of 0.03 \AA^{-1} , and (c) Q of 0.2 \AA^{-1} for the Longmaxi shale sample

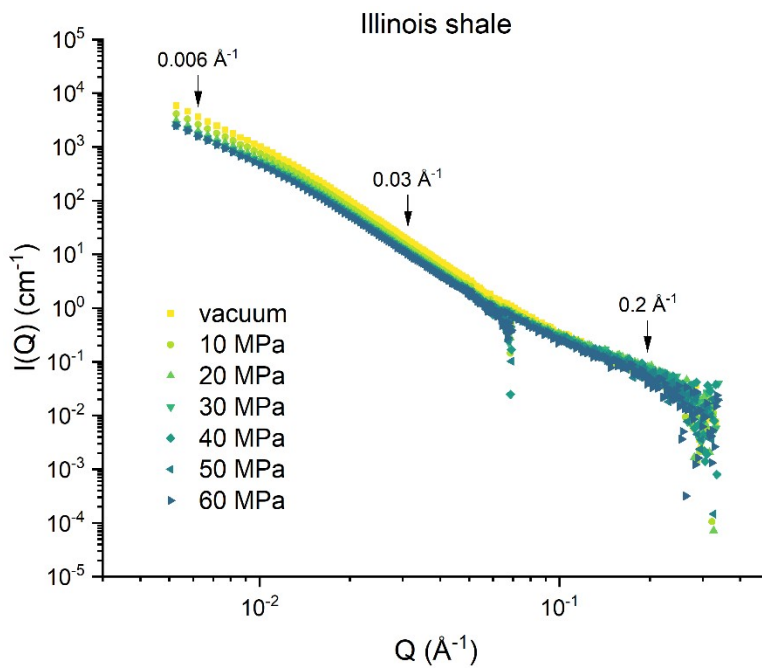


Figure S4 Scattering intensity as a function of methane pressure for the Illinois shale sample

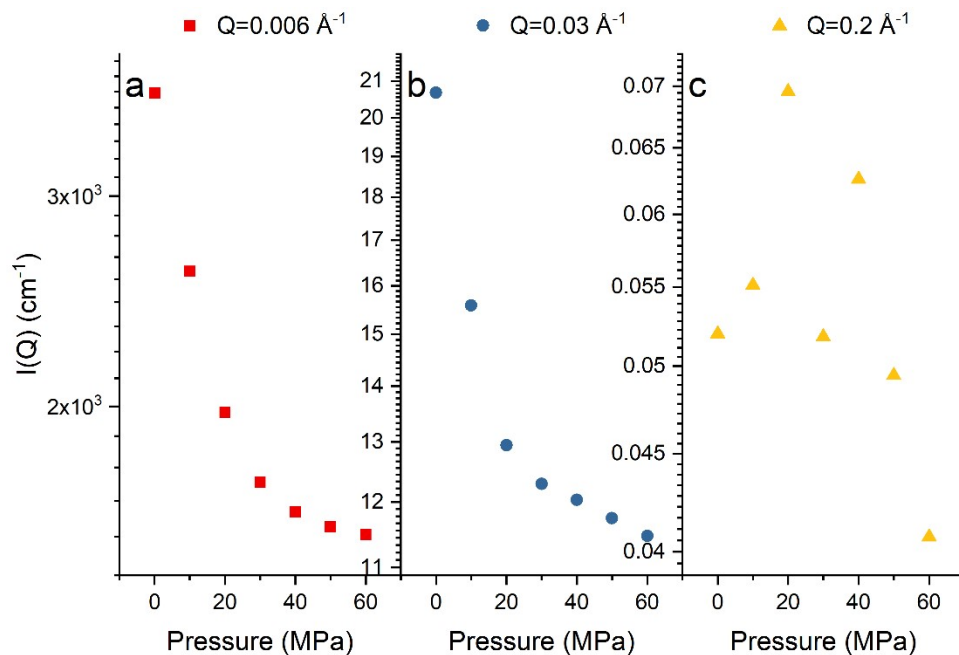


Figure S5 Scattering intensity as a function of methane pressure at (a) Q of 0.004 \AA^{-1} , (b) Q of 0.03 \AA^{-1} , and (c) Q of 0.2 \AA^{-1} for the Illinois shale sample

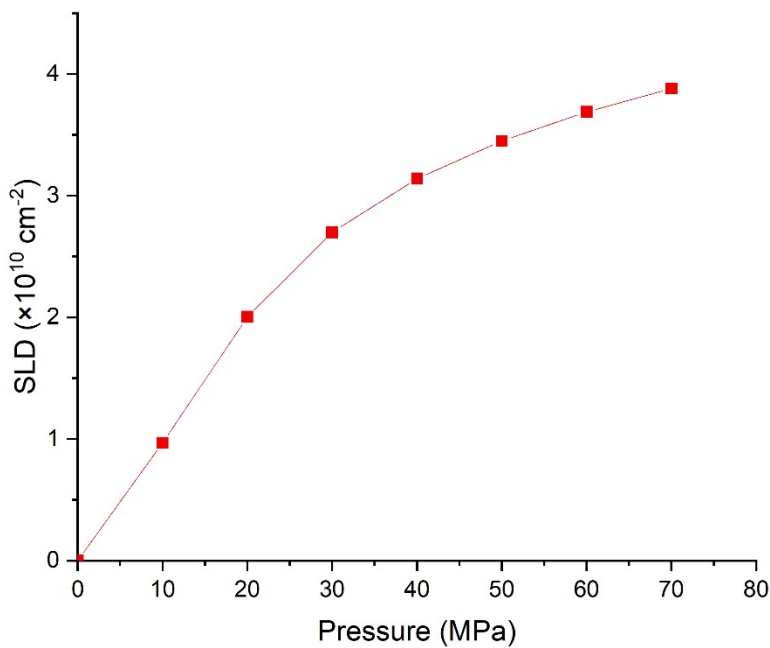


Figure S6 SLD of deuterated methane as a function of pressure

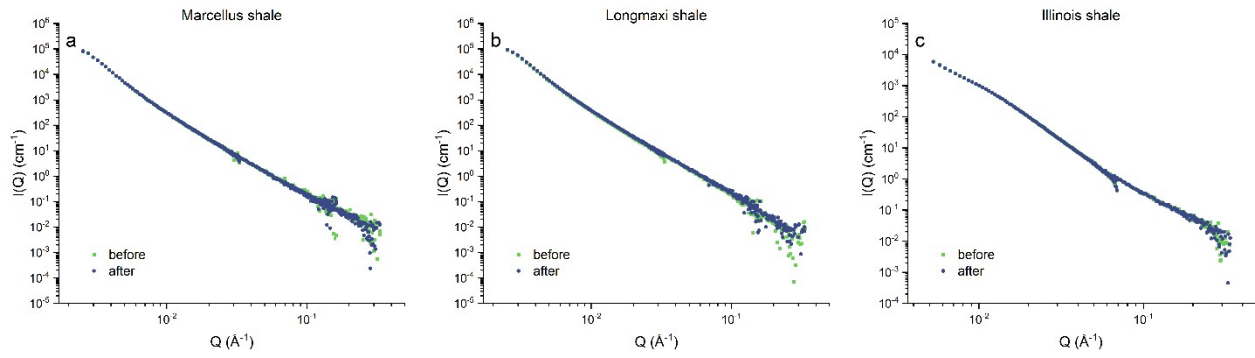


Figure S7 Scattering intensities under vacuum before and after CD_4 injection for the (a) Marcellus shale, (b) Longmaxi shale, and (c) Illinois shale samples

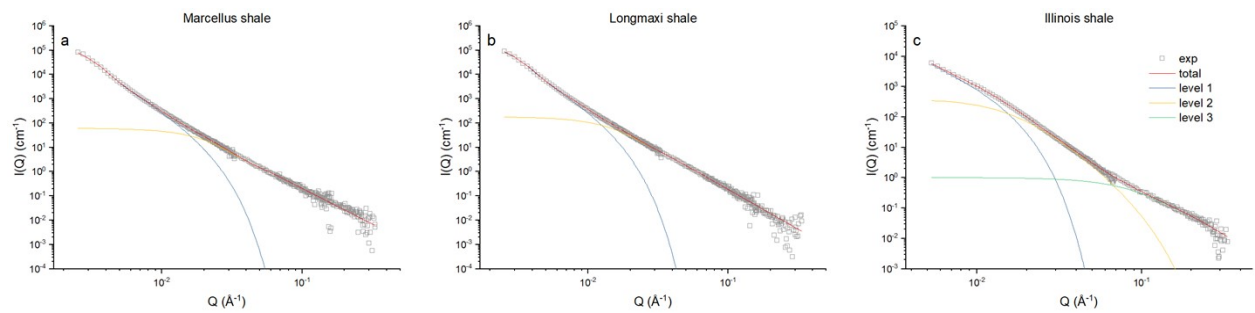


Figure S8 Model fitting using the unified scattering model for the scattering profiles of the (a) Marcellus shale, (b) Longmaxi shale, and (c) Illinois shale samples (scattering intensities under vacuum condition as examples)

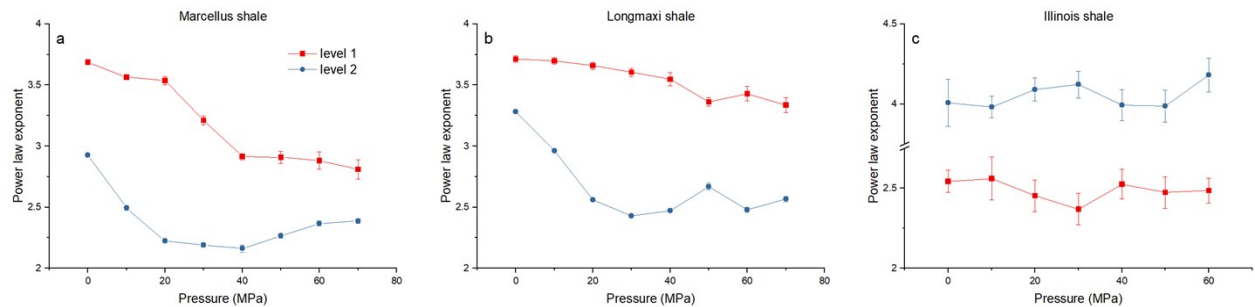


Figure S9 Power-law exponent as a function of pressure for the (a) Marcellus shale, (b) Longmaxi shale, and (c) Illinois shale samples

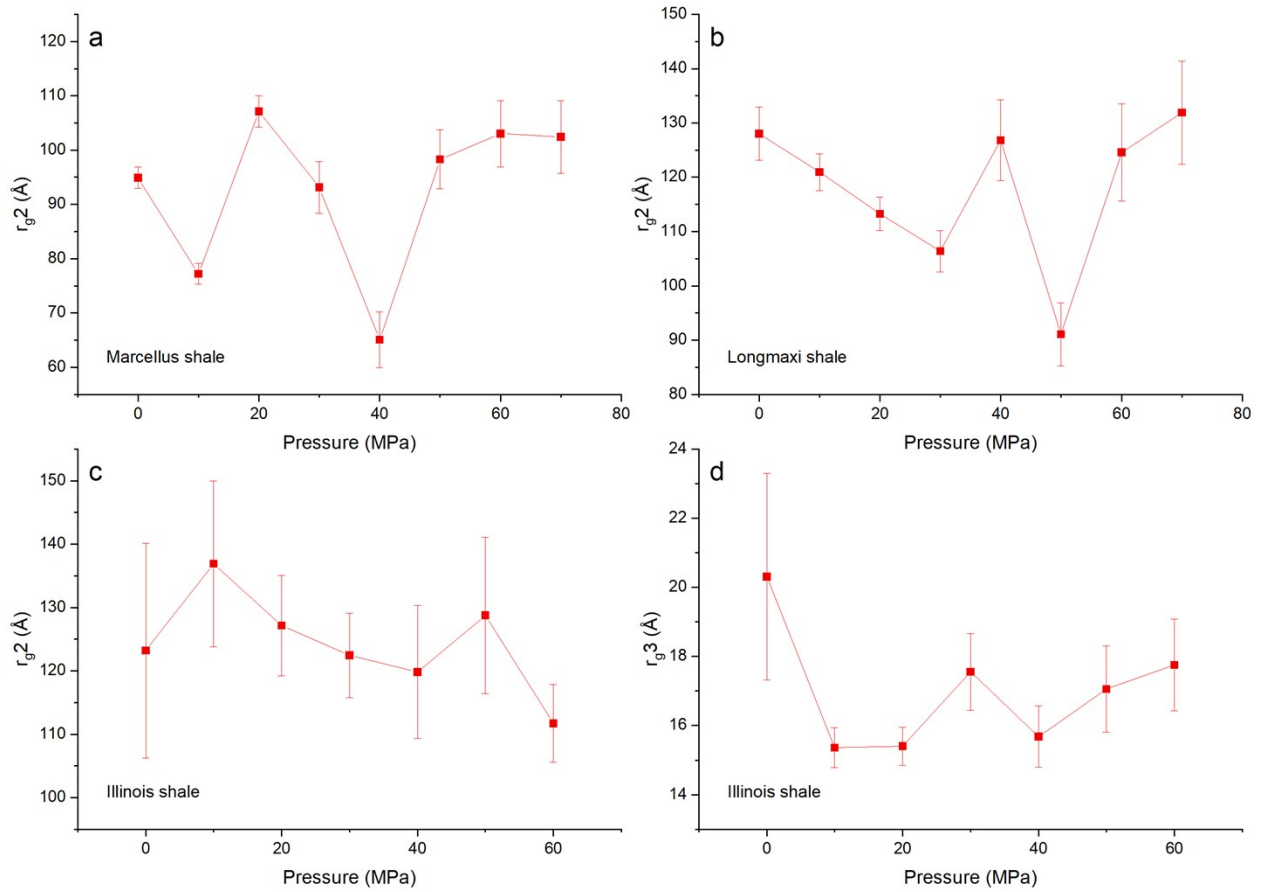


Figure S10 Radius of gyration as a function of pressure for the **(a)** Marcellus shale, **(b)** Longmaxi shale, and **(c) and (d)** Illinois shale samples

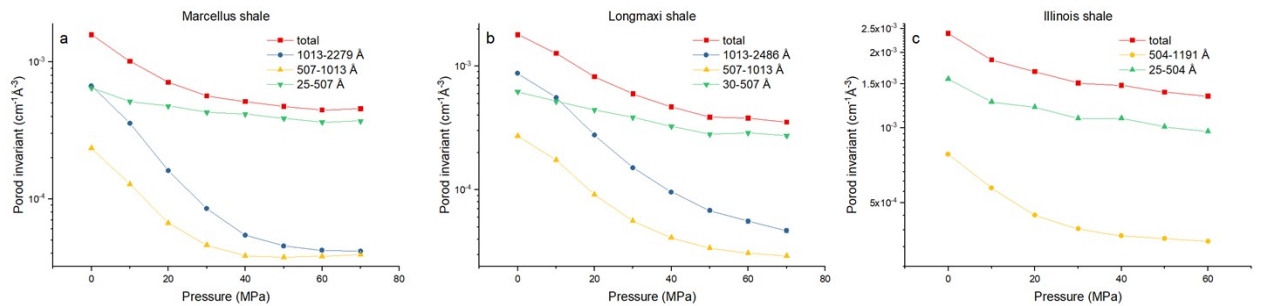


Figure S11 Porod invariant as a function of pressure for total and separated pore ranges for the **(a)** Marcellus shale, **(b)** Longmaxi shale, and **(c)** Illinois shale samples

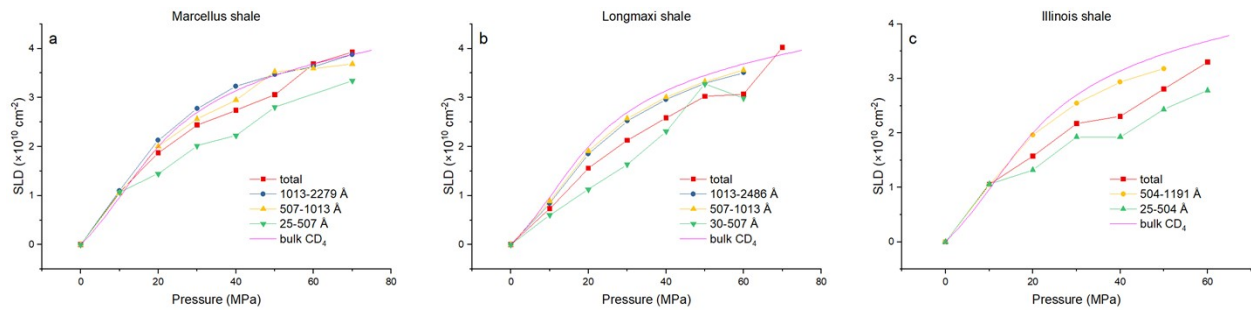


Figure S12 Average SLD in open pores as a function of pressure for total and separated pore ranges for the **(a)** Marcellus shale, **(b)** Longmaxi shale, and **(c)** Illinois shale samples

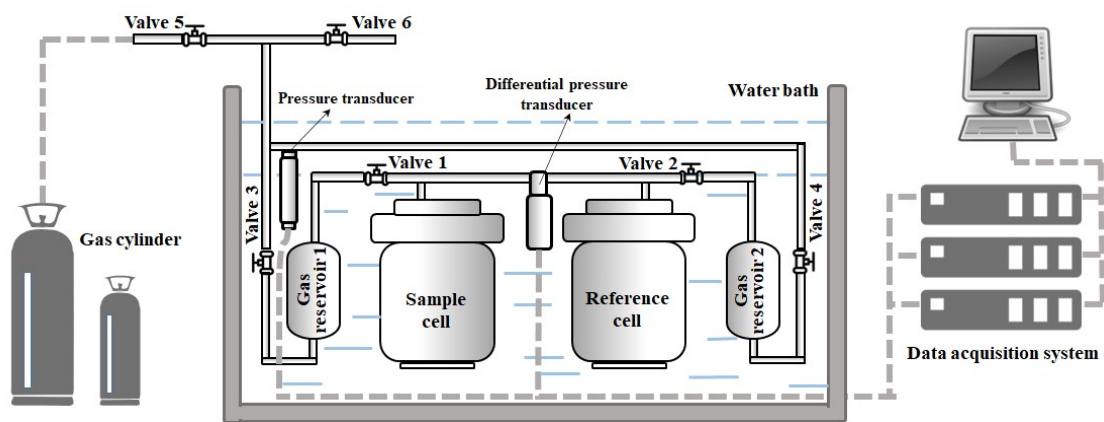


Figure S13 Schematic of the sorption experimental setup 7

Tables

Table S1 Chemical compositions and the effective SLDs of the shale samples^a

	Marcellus shale	Illinois shale	Longmaxi shale
quartz (wt.%)	72.68	4.91	49.82
calcite (wt.%)	/	/	19.36
muscovite (wt.%)	9.91	3.16	/
dolomite (wt.%)	/	/	16.35
pyrite (wt.%)	/	0.77	/
chlorite (wt.%)	/	16.70	/
glauconite (wt.%)	/	37.82	/
dickite (wt.%)	/	1.89	/
clinochlore (wt.%)	/	1.40	/
phengite (wt.%)	2.87	3.51	5.84
palygorskite (wt.%)	5.74	/	/
siderophyllite (wt.%)	/	/	5.93
karpatite (wt.%)	1.39	/	/
TOC (wt.%)	7.41	29.83	2.70
total (wt.%)	100	100	100
maturity R _o (%)	1.26	0.71	0.31
SLD ($\times 10^{10}$ cm ⁻²)	3.89	3.41	4.39

^aThe maturity of each sample is obtained from reference ⁷.

Table S2 The SLDs of deuterated methane under different pressure conditions^a

pressure (MPa)	gas density (g/cm ³)	SLD ($\times 10^{10}$ cm ⁻²)
0	0	0
10	0.097	0.97
20	0.200	2.00
30	0.270	2.70
40	0.314	3.14
50	0.345	3.45
60	0.368	3.69
70	0.388	3.88

^aThe temperature was 22°C.**Table S3** Model-fitting parameters for the Marcellus shale sample^a

pressure (MPa)	r_g1 (Å)	power1	B1 (cm ⁻¹)	G1 (cm ⁻¹)	r_g2 (Å)	power2	B2 (cm ⁻¹)	G2 (cm ⁻¹)
0	823.2(10.2)	3.687(0.019)	1.50E-05(1.31E-06)	3.18E+05(1.69E+04)	94.9(2.0)	2.926(0.013)	2.40E-04(8.41E-06)	62.36(4.30)
10	846.5(11.0)	3.565(0.016)	1.42E-05(1.06E-06)	1.99E+05(1.26E+04)	77.2(1.9)	2.493(0.019)	5.80E-04(2.63E-05)	19.61(1.49)
20	914.2(19.3)	3.537(0.035)	8.48E-06(1.44E-06)	1.18E+05(1.18E+04)	107.1(2.9)	2.224(0.014)	1.09E-03(3.71E-05)	33.30(3.06)
30	872.1(23.3)	3.211(0.037)	2.71E-05(4.86E-06)	4.56E+04(5.72E+03)	93.1(4.8)	2.192(0.017)	1.11E-03(4.51E-05)	16.47(2.67)
40	797.0(25.5)	2.914(0.024)	9.10E-05(1.04E-05)	1.79E+04(2.49E+03)	65.1(5.2)	2.162(0.028)	1.14E-03(6.93E-05)	5.35(1.23)
50	848.2(63.5)	2.909(0.050)	9.09E-05(2.29E-05)	1.67E+04(5.33E+03)	98.3(5.4)	2.265(0.018)	8.16E-04(3.65E-05)	18.07(3.46)
60	742.9(54.6)	2.882(0.071)	1.04E-04(3.70E-05)	8.95E+03(2.33E+03)	103.0(6.1)	2.366(0.018)	6.02E-04(2.84E-05)	21.49(4.60)

70	680.2(37.2)	2.809(0.078)	1.54E-04(5.99E-05)	6.68E+03(1.20E+03)	102.4(6.7)	2.387(0.019)	5.85E-04(2.92E-05)	21.74(5.26)
----	-------------	--------------	--------------------	--------------------	------------	--------------	--------------------	-------------

^aThe r_g1 may not be reasonable due to the limited low Q measured.

Table S4 Model-fitting parameters for the Longmaxi shale sample^a

pressure (MPa)	r_g1 (Å)	power1	B1 (cm ⁻¹)	G1 (cm ⁻¹)	r_g2 (Å)	power2	B2 (cm ⁻¹)	G2 (cm ⁻¹)
0	842.7(12.6)	3.713(0.026)	1.63E-05(2.02E-06)	3.74E+05(2.27E+04)	128.0(4.9)	3.282(0.011)	9.66E-05(2.84E-06)	184.30(23.69)
10	901.1(16.2)	3.697(0.027)	1.08E-05(1.41E-06)	3.23E+05(2.66E+04)	120.9(3.4)	2.960(0.011)	2.03E-04(6.01E-06)	107.89(10.16)
20	941.0(16.3)	3.659(0.028)	6.53E-06(9.12E-07)	1.92E+05(1.48E+04)	113.3(3.1)	2.562(0.012)	5.04E-04(1.58E-05)	52.65(4.56)
30	975.4(22.7)	3.604(0.032)	5.01E-06(7.94E-07)	1.18E+05(1.23E+04)	106.4(3.8)	2.429(0.014)	6.42E-04(2.27E-05)	30.95(3.19)
40	990.1(38.6)	3.546(0.054)	4.77E-06(1.29E-06)	7.20E+04(1.18E+04)	126.8(7.5)	2.472(0.014)	4.98E-04(1.83E-05)	38.76(6.65)
50	946.8(35.0)	3.362(0.034)	9.32E-06(1.57E-06)	4.04E+04(6.35E+03)	91.1(5.8)	2.670(0.028)	2.72E-04(1.85E-05)	14.45(2.18)
60	961.6(76.4)	3.429(0.060)	6.02E-06(1.82E-06)	3.02E+04(8.85E+03)	124.6(9.0)	2.479(0.018)	4.51E-04(2.10E-05)	30.40(5.89)
70	919.7(84.8)	3.336(0.062)	8.91E-06(2.79E-06)	1.98E+04(6.42E+03)	131.9(9.5)	2.567(0.021)	3.35E-04(1.85E-05)	33.31(6.39)

^aThe r_g1 may not be reasonable due to the limited low Q measured.

Table S5 Model-fitting parameters for the Illinois shale sample^a

pressure (MPa)	r_g1 (Å)	power1	B1 (cm ⁻¹)	G1 (cm ⁻¹)	r_g2 (Å)	power2	B2 (cm ⁻¹)	G2 (cm ⁻¹)	r_g3 (Å)	power3	B3 (cm ⁻¹)	G3 (cm ⁻¹)
0	534.7 (82.9)	2.544 (0.070)	1.06E-02 (3.41E-03)	4.23E+04 (2.09E+04)	123.2 (16.9)	4.008 (0.147)	2.08E-05 (8.77E-06)	403.02 (261.46)	20.3 (3.0)	3.305 (0.251)	2.97E-04 (1.01E-04)	1.01 (0.37)
10	539.5 (109.8)	2.561 (0.133)	6.88E-03 (4.59E-03)	2.82E+04 (1.76E+04)	136.9 (13.1)	3.981 (0.068)	1.56E-05 (3.21E-06)	503.58 (227.63)	15.4 (0.6)	7.843 (1.476)	7.38E-07 (1.39E-06)	0.53 (0.04)
20	511.5 (89.0)	2.453 (0.098)	9.34E-03 (4.13E-03)	1.77E+04 (8.67E+03)	127.2 (7.9)	4.091 (0.072)	9.23E-06 (2.02E-06)	284.32 (78.482)	15.4 (0.5)	6.341 (0.943)	7.94E-06 (9.41E-06)	0.58 (0.04)

30	527.5 (93.4)	2.370 (0.099)	1.22E-02 (5.48E-03)	1.75E+04 (9.57E+03)	122.4 (6.7)	4.121 (0.084)	8.04E-06 (2.05E-06)	212.17 (51.06)	17.6 (1.1)	4.987 (0.746)	3.13E-05 (3.10E-05)	0.69 (0.08)
40	495.5 (83.3)	2.526 (0.092)	5.41E-03 (2.24E-03)	1.35E+04 (6.05E+03)	119.8 (10.5)	3.993 (0.098)	1.20E-05 (3.48E-06)	205.34 (79.915)	15.7 (0.9)	5.161 (0.920)	3.63E-05 (4.17E-05)	0.53 (0.05)
50	530.8 (99.7)	2.474 (0.099)	6.47E-03 (3.08E-03)	1.65E+04 (9.72E+03)	128.8 (12.3)	3.987 (0.101)	1.18E-05 (3.59E-06)	268.62 (115.23)	17.1 (1.2)	5.184 (0.943)	2.17E-05 (2.67E-05)	0.58 (0.08)
60	509.1 (71.5)	2.485 (0.078)	6.16E-03 (2.17E-03)	1.51E+04 (6.35E+03)	111.7 (6.1)	4.181 (0.107)	6.57E-06 (2.10E-06)	143.24 (33.747)	17.8 (1.3)	5.452 (1.003)	1.16E-05 (1.57E-05)	0.63 (0.09)

^aThe r_{g1} may not be reasonable due to the limited low Q measured, and the power3 under gas injection is not reasonable due to the high uncertainties at high Q.

Table S6 Volume fractions and average pore accessibility for the three shale samples

	Marcellus shale	Longmaxi shale	Illinois shale
open pores, ϕ_o	0.046	0.058	0.041
closed pores, ϕ_c	0.017	0.013	0.046
pore accessibility, C_{ac}	0.731	0.821	0.467

Table S7 Pearson correlation analysis

Pearson correlations	TOC	maturity	contrast-matched SLD	total pores	pore accessibility
TOC	1	0.0722	0.94482	0.89373	-0.99645
maturity	0.0722	1	-0.25853	-0.3829	-0.15589
contrast-matched SLD	0.94482	-0.25853	1	0.99137	-0.91389
total pores	0.89373	-0.3829	0.99137	1	-0.85281
pore accessibility	-0.99645	-0.15589	-0.91389	-0.85281	1

Table S8 Contrast-matched pressure and SLD for total and different pore ranges

Marcellus shale			Longmaxi shale			Illinois shale		
pore range (Å)	pressure (MPa)	SLD ($\times 10^{10} \text{ cm}^{-2}$)	pore range (Å)	pressure (MPa)	SLD ($\times 10^{10} \text{ cm}^{-2}$)	pore range (Å)	pressure (MPa)	SLD ($\times 10^{10} \text{ cm}^{-2}$)
total	60.000	3.69	total	61.842	3.73	total	71.111	3.90
1013-2279	64.718	3.78	1013-2486	71.915	3.91	/	/	/
507-1013	44.596	3.29	507-1013	68.786	3.86	504-1191	63.533	3.76
25-507	75.436	3.97	30-507	65.991	3.81	25-504	104.061	4.35

References

1. S. Lee, T. B. Fischer, M. R. Stokes, R. J. Klingler, J. Ilavsky, D. K. McCarty, M. O. Wigand, A. Derkowski and R. E. Winans, Dehydration effect on the pore size, porosity, and fractal parameters of shale rocks: Ultrasmall-angle X-ray scattering study, *Energy & Fuels*, 2014, **28**, 6772-6779.
2. Y. Wang, Y. Qin, R. Zhang, L. He, L. M. Anovitz, M. Bleuel, D. F. R. Mildner, S. Liu and Y. Zhu, Evaluation of Nanoscale Accessible Pore Structures for Improved Prediction of Gas Production Potential in Chinese Marine Shales, *Energy & Fuels*, 2018, **32**, 12447-12461.
3. <http://www.sasview.org/>.
4. G. Beaucage, Approximations leading to a unified exponential power-law approach to small-angle scattering, *Journal of Applied Crystallography*, 1995, **28**, 717-728.
5. R. Zhang, S. Liu and Y. Wang, Fractal evolution under in situ pressure and sorption conditions for coal and shale, *Scientific Reports*, 2017, **7**, 8971.
6. A. P. Radlinski, Small-angle neutron scattering and the microstructure of rocks, *Rev Mineral Geochem*, 2006, **63**, 363-397.
7. L. Fan and S. Liu, A novel experimental system for accurate gas sorption and its application to various shale rocks, *Chemical Engineering Research and Design*, 2021, **165**, 180-191.